Comp. Appl. Math. (2017) 36:971–990
DOI 10.1007/s40314-015-0273-9

Three types of meshless finite volume method for the analysis of two-dimensional elasticity problems

M. Ebrahimnejad[1] · N. Fallah[1] · A. R. Khoei[2]

Received: 19 September 2014 / Revised: 20 August 2015 / Accepted: 24 August 2015 /
Published online: 15 September 2015

Abstract This paper presents three schemes of 2D meshless finite volume (MFV) method, referred to as MFV with overlapping control volumes (MFV1), MFV with irregular non-overlapping control volumes (MFV2) and MFV with regular non-overlapping control volumes (MFV3). The methods utilize the local symmetric weak form of system equation and the interpolation functions constructed using the weighted multi-triangles method (WMTM) which is recently developed by the present authors. The proposed formulation involves only integrals over the boundaries of control volumes. The performance of the proposed schemes is studied in three benchmark problems. A comparative study between the predictions of the above MFV schemes and finite element method (FEM) shows the superiority of WMTM-based MFV1 and MFV2 over FEM.

Keywords Finite volume method · Meshless methods · Control volume (CV) · Interpolation function

Mathematics Subject Classification Primary 74S10 · Secondary 74-02

1 Introduction

Meshless methods have become very popular numerical tools for solving mechanical problems. These methods rely on a set of scattered nodes to discretize the problem domain and no element or connectivity of the nodes is needed. Therefore, they have certain advantages

Communicated by Domingo Alberto Tarzia.

M. Ebrahimnejad—PhD candidate.

✉ N. Fallah
fallah@guilan.ac.ir

[1] Department of Civil Engineering, University of Guilan, Rasht, Iran

[2] Department of Civil Engineering, Sharif University of Technology, Tehran, Iran

compared with the conventional mesh-based finite element method (FEM). The main objective of the meshless methods is to eliminate or reduce the difficulties associated with FEM such as the meshing and re-meshing difficulties, locking, discontinuities in crack modeling and element distortions in problems with large deformations.

In the last two decades, considerable research has been performed to develop the meshless methods such as element-free Galerkin (EFG) (Belytschko et al. 1994), smoothed particle hydrodynamics (SPH) (Liu and Liu 2003), finite point method (FPM) (Oñate et al. 1996), reproducing kernel particle method (RKPM) (Liu et al. 1995; Khoei et al. 2007) , meshless local Petrov–Galerkin (MLPG) (Atluri and Zhu 1998) method and meshless methods based on Peridynamics formulation (Silling et al. 2007; Ganzenmüller et al. 2015). Some of these methods, despite their advantages, involve some undermining issues such as the high computational cost, singularity of moment matrix, imposition of essential boundary conditions and selection of effective parameters such as the size of nodal influence domain and local quadrature domain.

In recent years, the MFV method has been applied for analyzing a wide variety of problems including elasto-static (Atluri and Shen 2002; Atluri et al. 2004; Han and Atluri 2004a; Moosavi et al. 2011), elasto-dynamic (Han and Atluri 2004b), beam (Raju and Phillips 2003), thick plate (Qian et al. 2003), shell (Moosavi et al. 2012a) and crack problems (Moosavi et al. 2012b) . In the above-mentioned studies, the overlapping circular or rectangular quadrature domains are used which can produce some difficulties and inaccuracy, especially in problems with complex shapes and irregular nodal distributions. One way to avoid this problem is benefiting from the patterns used in the conventional finite volume (FV) method to construct the control volumes (CVs). In fact, the main motivation for developing the new MFV schemes in this paper is to unify the advantages of meshless methods and FV technique. Meshless methods are flexible, because there is no need for any mesh. Furthermore, these methods rectify some of the disadvantages of mesh-based methods such as discontinuous secondary variables across the inter-element boundaries and the need for re-meshing in large deformation problems. Moreover, the conventional FV method, which has been used for analyzing the stresses in elasticity problems (Bailey and Cross 1995; Wheel 1996), beams (Fallah and Hatami 2006), plates (Wheel 1997; Fallah 2004, 2006), large deformations (Maneeratana 2000; Fallah et al. 2000), elasto-plasticity (Demirdzic and Martinovic 1993; Taylor et al. 2003; Fallah and Paryandeh-Shahrestany 2014), dynamic fracture problems (Ivankovic et al. 1994; Stylianou and Ivankovic 2002), shallow water flow (Sabbagh-Yazdi and Mohammadzadeh-Qomi 2004) and dynamics (Slone et al. 2003; Fallah and Ebrahimnejad 2014), is able to compete with FEM in terms of numerical accuracy and computational efficiency.

In this paper, three MFV schemes are introduced. In MFV with overlapping CVs (MFV1), the FV cell centered scheme (Fallah 2004) is adopted in which the rectangular CVs are formed around the field nodes. In MFV with irregular non-overlapping CVs (MFV2), CVs are constructed according to the FV cell vertex scheme (Fallah 2004). By doing so, the choice of control volumes, particularly in complex geometries, becomes straightforward. In MFV with regular non-overlapping CVs (MFV3), the regular background cells are used as the CVs. In fact, there is no correspondence between node locations and CVs construction in this scheme; therefore, nodes can be placed at any positions according to the analyst desires.

In the above proposed MFV schemes, a new interpolation method referred to as weighted multi-triangles method (WMTM) developed by the present authors (Ebrahimnejad et al. 2014) is used. WMTM can enhance the performance of MFV schemes by resolving the problematic issues such as ill conditioning, enforcing the essential boundary conditions, computational cost, selection of some effective parameters such as weighting function and average nodal distance especially in problems with irregular nodal distribution, which are the common issues

in methods like the well-known moving least squares (MLS) approximation. To demonstrate the performance of the presented WMTM-based MFV schemes, some benchmark problems are investigated.

The organization of the rest of this paper is as follows: In Sect. 2, a brief discussion of WMTM for construction of approximation functions is presented. Discretization of the governing equations using MFV is presented in Sect. 3, by introducing three different schemes. Section 4 demonstrates the effectiveness of the proposed schemes by analyzing the numerical results of some benchmark problems. Finally, conclusions are presented in Sect. 5.

2 Weighted multi-triangles method (WMTM)

In this work, the approximating functions and their derivatives corresponding to a point of interest are obtained using the weighted multi-triangles method (WMTM) (Ebrahimnejad et al. 2014). In this technique, first of all, the first layer of neighbor nodes for a point of interest, p, is determined locally using the Delaunay triangulation, where the desired point is the common vertex of the patch of triangles. These neighbor nodes are the vertices of the surrounding region that houses the desired point, p, see Fig. 1a. Then, a series of triangles housing the point, p, are made using the vertices of the polygon (i.e. neighbor field nodes), Fig. 1b. In the WMTM, contribution of each vertex of the surrounding triangles in the construction of interpolation function is modified according to its distance from the desired point, p, by applying the weighting parameter $1/r^{\lambda}$. In each triangle, the field variable on p, i.e. $\bar{u}_p$, can be approximated as follows

$$\bar{u}_p = R_1\bar{u}_1 + R_2\bar{u}_2 + R_3\bar{u}_3 \tag{1}$$

where

$$\begin{aligned} &R_1 = \frac{\psi_1}{\sum_i \psi_i}, R_2 = \frac{\psi_2}{\sum_i \psi_i}, R_3 = \frac{\psi_3}{\sum_i \psi_i} \\ &\psi_1 = \delta_1\left(\frac{1}{r_1^{\lambda}}\right), \psi_2 = \delta_2\left(\frac{1}{r_2^{\lambda}}\right), \psi_3 = \delta_3\left(\frac{1}{r_3^{\lambda}}\right) \\ &\delta_1 = \frac{A_1}{A}, \delta_2 = \frac{A_2}{A}, \delta_3 = \frac{A_3}{A}; |\lambda| \le 0.05 \\ &A = A_1 + A_2 + A_3 \end{aligned} \tag{2}$$

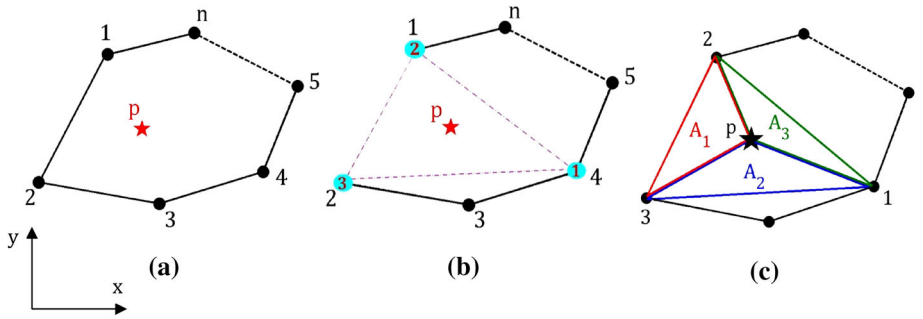

Fig. 1 Surrounding nodes and multi-triangles corresponding to the desired point, p

where λ is a constant that controls the smoothness of the interpolation function, r_i represents the distance from the desired point p to the ith vertex of the surrounding triangle, $\delta_1, \delta_2, \delta_3$ are the local interpolation functions for each surrounding triangle and A_1, A_2, A_3 are shown in Fig. 1c.

According to Fig. 1a, for a surrounding polygon with n nodes, (1) can be rewritten for a typical triangle l consisting of nodes i, j, m in the form of

$$\bar{u}_{p,l} = \sum_{k=1}^{n} \mu_{k,l} \bar{u}_k \tag{3}$$

where $\mu_{k,l}$ is the interpolation function of node k of the triangle l with the following properties

$$\mu_{i,l} = R_1, \mu_{j,l} = R_2, \mu_{m,l} = R_3 \tag{4a}$$

and

$$\mu_{k,l} = 0 \quad \text{for } k \neq i, \ j, \ m \tag{4b}$$

Finally, the field variable in the desired point p, u_p, is approximated in terms of the field variables associated with the surrounding field nodes by averaging the local approximations $\bar{u}_{p,l}$ corresponding to n surrounding triangles as follows

$$u_p = \frac{1}{n} \sum_{l=1}^{n} \bar{u}_{p,l} = \frac{1}{n} \sum_{l=1}^{n} \sum_{k=1}^{n} \mu_{k,l} \bar{u}_k = \sum_{k=1}^{n} \left(\frac{1}{n} \sum_{l=1}^{n} \mu_{k,l} \right) \bar{u}_k = \sum_{k=1}^{n} \phi_k \bar{u}_k \tag{5}$$

where ϕ_k represents the approximating function corresponding to the field node k as

$$\phi_k = \frac{1}{n} \sum_{l=1}^{n} \mu_{k,l}, \quad k = 1, 2, \ldots, n \tag{6}$$

Accordingly, the first derivatives of approximating function ϕ_k can be obtained as follows

$$(\phi_k)_{,x} = \frac{1}{n} \sum_{l=1}^{n} (\mu_{k,l})_{,x}; \ (\phi_k)_{,y} = \frac{1}{n} \sum_{l=1}^{n} (\mu_{k,l})_{,y} \tag{7}$$

It should be noted that the WMTM interpolation functions possess the characteristics such as partition of unity, Kronecker delta function, linear reproducing and continuity at all orders, as shown by Ebrahimnejad et al. (2014). Furthermore, there is no need for the additional parameters such as weight functions and dimension of support domain for constructing the interpolation functions, those to be selected in MLS method based on the numerical experiments. Moreover, the scheme introduced in this technique for selecting the field nodes reduces the number of influencing nodes for the points of interest and consequently reduces the numerical efforts. This is highly desirable especially for problems with high-density node distribution.

3 Discretization of governing equations using MFV

In the meshless finite volume (MFV) technique, the weighted residual method is used for deriving the weak form of equilibrium equations for each CV corresponding to the field nodes. The equilibrium equations for a CV in a 2D elastic solid are written as

$$\mathbf{L}^{\mathrm{T}}\boldsymbol{\sigma} + \mathbf{b} = 0 \tag{8}$$

where $\boldsymbol{\sigma}$ and $\mathbf{b}$ represent stress and body force vectors, respectively, and differential operator $\mathbf{L}$ is defined as follows

$$\mathbf{L} = \begin{bmatrix} \frac{\partial}{\partial x} & 0 \\ 0 & \frac{\partial}{\partial y} \\ \frac{\partial}{\partial y} & \frac{\partial}{\partial x} \end{bmatrix} \tag{9}$$

The boundary conditions are given as

$$\begin{aligned} &\mathbf{u} = \bar{\mathbf{u}} \quad \text{on the essential boundaries } \Gamma_u \\ &\mathbf{t} = \mathbf{n}\boldsymbol{\sigma} = \bar{\mathbf{t}} \quad \text{on the natural boundaries } \Gamma_t \end{aligned} \tag{10}$$

where $\mathbf{u}$ represents the displacement vector, $\bar{\mathbf{u}}$ and $\bar{\mathbf{t}}$ are the prescribed displacements and tractions, respectively, and $\mathbf{n}$ contains the components of unit outward normal to the boundaries of CV as

$$\mathbf{n} = \begin{bmatrix} n_x & 0 & n_y \\ 0 & n_y & n_x \end{bmatrix} \tag{11}$$

For a considered CV, the weighted residual method can be written in the following form

$$\int_{\Omega_{\mathrm{cv}}} \widehat{\mathbf{W}}(\mathbf{L}^{\mathrm{T}}\boldsymbol{\sigma} + \mathbf{b})\mathrm{d}\Omega - \alpha \int_{\Gamma_u} \widehat{\mathbf{W}}(\mathbf{u} - \bar{\mathbf{u}})\mathrm{d}\Gamma = 0 \tag{12}$$

where Ω_{cv} represents the area of control volume, Γ_u is the part of the global essential boundary that intersects the Ω_{cv}, $\widehat{\mathbf{W}}$ is the weighting function and α is the penalty factor.

Using the divergence theorem, (12) can be rewritten as

$$\int_{\Gamma} \widehat{\mathbf{W}}(\mathbf{n}\boldsymbol{\sigma})\mathrm{d}\Gamma - \int_{\Omega_{\mathrm{cv}}} (\mathbf{L}\widehat{\mathbf{W}})^{\mathrm{T}}\boldsymbol{\sigma}\mathrm{d}\Omega + \int_{\Omega_{\mathrm{cv}}} \widehat{\mathbf{W}}\mathbf{b}\mathrm{d}\Omega - \alpha \int_{\Gamma_u} \widehat{\mathbf{W}}(\mathbf{u} - \bar{\mathbf{u}})\mathrm{d}\Gamma = 0 \tag{13}$$

To achieve the MFV discretized equations, the Heaviside function is used as the weighting function, i.e.

$$\begin{cases} \widehat{\mathbf{W}} = I & \text{over } \Omega_{\mathrm{cv}} \\ \widehat{\mathbf{W}} = 0 & \text{elsewhere} \end{cases} \tag{14}$$

Consequently

$$\mathbf{L}\widehat{\mathbf{W}} = 0 \tag{15}$$

Equation (15) leads to simplicity in formulation by removing a domain integral over Ω_{cv} in (13). It is expected that the reduction of computational cost is achieved due to use of only line integrations in deriving the stiffness matrix.

The first line integral of (13) can be divided into integrals on internal boundary Γ_0, local essential boundary Γ_u and local natural boundary Γ_t, since Γ is the union of above-mentioned three parts (i.e. $\Gamma = \Gamma_0 \cup \Gamma_u \cup \Gamma_t$). Therefore, using (15), Eq. (13) can be written as

$$-\int_{\Gamma_0} \mathbf{n}\boldsymbol{\sigma}\mathrm{d}\Gamma - \int_{\Gamma_u} \mathbf{n}\boldsymbol{\sigma}\mathrm{d}\Gamma - \int_{\Gamma_t} \mathbf{n}\boldsymbol{\sigma}\mathrm{d}\Gamma = \int_{\Omega_{\mathrm{cv}}} \mathbf{b}\mathrm{d}\Omega - \alpha \int_{\Gamma_u} (\mathbf{u} - \bar{\mathbf{u}})\mathrm{d}\Gamma \tag{16}$$

Using the constitutive equation, the stress components can be stated in terms of the strain components in the following form

$$\boldsymbol{\sigma} = \mathbf{D}\boldsymbol{\varepsilon} \tag{17}$$

where $\mathbf{D}$ is the elasticity matrix. The strain field consists of the strain-displacement relation and is presented as follows

$$\boldsymbol{\varepsilon} = \mathbf{Lu} \tag{18}$$

Substituting (10), (17) and (18) into (16) gives

$$-\int_{\Gamma_0} \mathbf{nDLu}\,\mathrm{d}\Gamma - \int_{\Gamma_u} \mathbf{nDLu}\,\mathrm{d}\Gamma = \int_{\Omega_{\mathrm{cv}}} \mathbf{b}\,\mathrm{d}\Omega + \int_{\Gamma_t} \bar{\mathbf{t}}\mathrm{d}\Gamma - \alpha \int_{\Gamma_u} (\mathbf{u} - \bar{\mathbf{u}})\mathrm{d}\Gamma \tag{19}$$

In the proposed MFV formulation, the unknown displacement $\mathbf{u}$ can be approximated by using the WMTM interpolation functions in terms of the nodal parameter $\widehat{\mathbf{u}}$ as follows

$$\mathbf{u} = \boldsymbol{\phi}\widehat{\mathbf{u}} \tag{20}$$

where the entries of $\boldsymbol{\phi}$ are WMTM interpolation functions. Substituting (20) into (19) results in

$$-\int_{\Gamma_0} \mathbf{nDL}\boldsymbol{\phi}\widehat{\mathbf{u}}\,\mathrm{d}\Gamma - \int_{\Gamma_u} \mathbf{nDL}\boldsymbol{\phi}\widehat{\mathbf{u}}\,\mathrm{d}\Gamma + \alpha \int_{\Gamma_u} \boldsymbol{\phi}\widehat{\mathbf{u}}\,\mathrm{d}\Gamma = \int_{\Omega_{\mathrm{cv}}} \mathbf{b}\,\mathrm{d}\Omega + \int_{\Gamma_t} \bar{\mathbf{t}}\mathrm{d}\Gamma + \alpha \int_{\Gamma_u} \bar{\mathbf{u}}\,\mathrm{d}\Gamma \tag{21}$$

Equation (21) presents two linear equilibrium equations of forces acting on a CV which can be written as

$$\mathbf{k}\widehat{\mathbf{u}} = \mathbf{f} \tag{22a}$$

where

$$\begin{aligned} \mathbf{k} &= -\int_{\Gamma_0} \mathbf{nDL}\boldsymbol{\phi}\,\mathrm{d}\Gamma - \int_{\Gamma_u} \mathbf{nDL}\boldsymbol{\phi}\,\mathrm{d}\Gamma + \alpha \int_{\Gamma_u} \boldsymbol{\phi}\,\mathrm{d}\Gamma \\ \mathbf{f} &= \int_{\Omega_{\mathrm{cv}}} \mathbf{b}\,\mathrm{d}\Omega + \int_{\Gamma_t} \bar{\mathbf{t}}\,\mathrm{d}\Gamma + \alpha \int_{\Gamma_u} \bar{\mathbf{u}}\,\mathrm{d}\Gamma \end{aligned} \tag{22b}$$

Equation (22a) can be written for all the CVs of the model, providing a set of simultaneous linear equations which can be stated in the compact form as

$$\mathbf{KU} = \mathbf{F} \tag{23}$$

where $\mathbf{K}$, $\mathbf{F}$ and $\mathbf{U}$ are the global stiffness matrix, global force vector and global displacement vector, respectively.

3.1 MFV with overlapping CVs (MFV1)

The above-mentioned formulation can be extended for any node-based interpolation functions and also for CVs with arbitrary sizes and shapes, including overlapping/non-overlapping CVs. This is the main advantage of MFV technique in comparison with the conventional FV method.

In MFV1 scheme, first, the filed nodes are distributed in the problem domain and then, the regular CVs (rectangular or circular CVs in 2D problems) are formed around them; see Fig. 2. The sizes of CVs are controlled with an additional parameter called dimensionless size of CV, which is problem-dependent and selected using the numerical experiments. The CVs

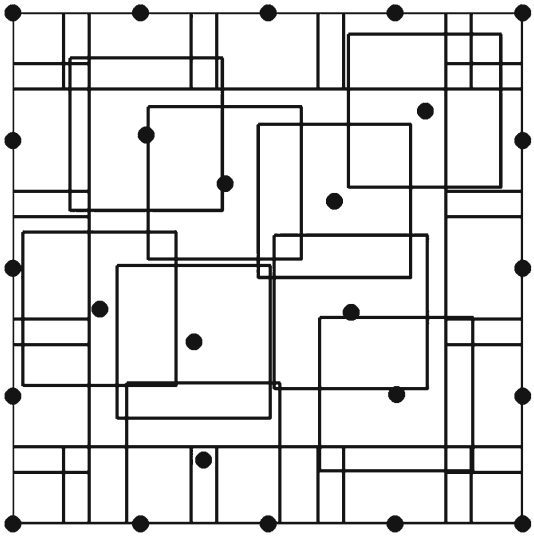

Fig. 2 Schematics of MFV1 scheme

produced by this scheme will be overlapped ones, especially in the cases with the irregular node distribution.

It has been shown that the computational cost in MFV1 applications is lower than or at least comparable to FEM. Therefore, MFV1 can provide a simple and efficient alternative to the finite element and boundary element methods for engineering analysis (Atluri and Shen 2002).

3.2 MFV with irregular non-overlapping CVs (MFV2)

In problems with complex geometries or with irregular distributed nodes, trial and error is required for constructing the appropriate regular non-overlapping CVs. One way to avoid this issue is the use of MFV2 scheme; a method similar to the cell vertex scheme of the conventional FV (Fallah 2004). In this scheme, the non-overlapping polygonal CVs are formed around the distributed field nodes. In doing so, first, using the Delaunay triangulation scheme, a mesh of triangles is made in which, the field nodes are used as the vertices of the triangles. Then, CVs are constructed corresponding to each field node by connecting the centers of surrounding triangles to the middle of their sides passing the field nodes; see Fig. 3. Unlike the conventional FV method in which the construction of the interpolation functions is based on the considered mesh, the triangular mesh made by the Delaunay triangulation is only for the CVs construction purposes and it is dumped thereafter. In other words, construction of the interpolation functions on any desired point is only based on the location of neighbor nodes.

3.3 MFV with regular non-overlapping CVs (MFV3)

In MFV1 and MFV2 schemes presented in the previous sections, field nodes are located at the center of the CVs. In the third scheme of MFV referred as MFV3, a background mesh covering the field problem can be used as the non-overlapping CVs regardless of field nodes distribution. In other words, since in MFV formulation the equilibrium equations are written

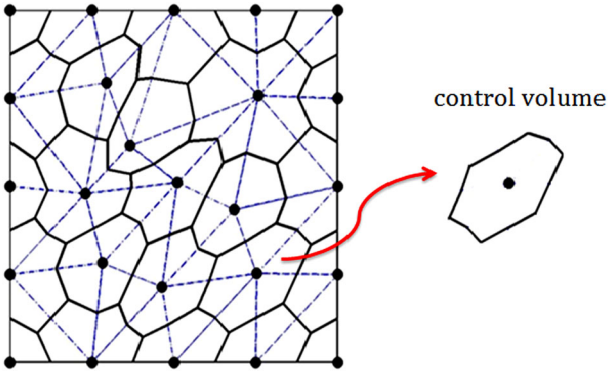

Fig. 3 Schematics of MFV2 scheme

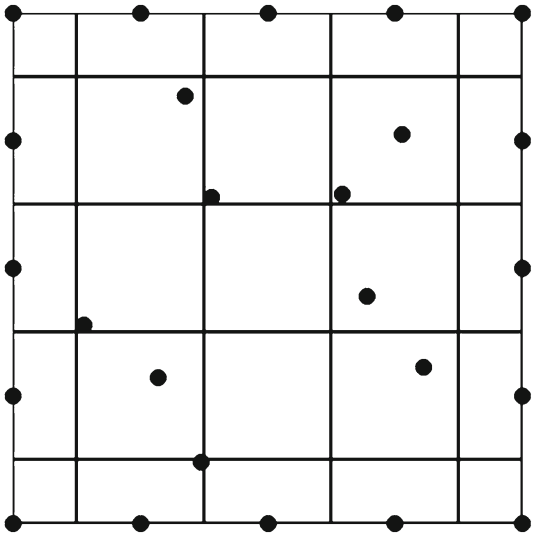

Fig. 4 Schematics of MFV3 scheme

for the CVs, there is no need to place field nodes at the center of CVs and they can be at any position, whether inside or outside the CVs; see Fig. 4. These CVs are somehow similar to the background mesh in the EFG method (Belytschko et al. 1994), except that in MFV3 the equilibrium is satisfied in an average sense locally and also the number of CVs must be equal to the number of field nodes. It should be noted that, in MFV3 scheme some field nodes should be placed on the natural and essential boundaries to ensure that the boundary conditions are properly considered in the formulation.

It is noticeable that in MFV3 scheme the CVs are consistent with the geometry of problem domain. Since the interpolation functions depend only on the location of field nodes and are independent of the geometry of CVs, therefore, MFV3 scheme is considered as a meshless method.

4 Numerical examples

In this section, three benchmark plane stress problems are considered to evaluate the accuracy and effectiveness of the proposed MFV schemes. The linear elastic analysis under small deformation is implemented in the MATLAB software environment. For the comparison purposes, in addition to the exact results, an in-house MATLAB code for FE analysis is developed and the results of FEM using the four-node quadrilateral elements (Q4) and full integration are presented.

In MFV1 scheme, the rectangular CVs with dimensions of $L_x = 1.1d_x$ and $L_y = 1.1d_y$ are used, where d_x and d_y are the average nodal distance in x and y directions, respectively. In the following examples, 2-points Gaussian quadrature rule is adopted to calculate the integrals. Also, the direct method is used to solve the linear system of algebraic equations.

The comparison of the results is accomplished based on the relative displacement and energy error norms, which are defined as

$$e_d = \frac{||\boldsymbol{u}^{\text{exact}} - \boldsymbol{u}^{\text{MFV}}||}{||\boldsymbol{u}^{\text{exact}}||}$$
$$e_e = \frac{||\boldsymbol{\varepsilon}^{\text{exact}} - \boldsymbol{\varepsilon}^{\text{MFV}}||}{||\boldsymbol{\varepsilon}^{\text{exact}}||} \tag{24}$$

where

$$||\boldsymbol{u}|| = \left(\int_{\Omega} \boldsymbol{u}^T \cdot \boldsymbol{u} \mathrm{d}\Omega \right)^{\frac{1}{2}}$$
$$||\boldsymbol{\varepsilon}|| = \left(\int_{\Omega} \boldsymbol{\varepsilon}^T \cdot \boldsymbol{c} \cdot \boldsymbol{\varepsilon} \mathrm{d}\Omega \right)^{\frac{1}{2}}. \tag{25}$$

4.1 Cantilever beam

In this example, the convergence of MFV schemes is investigated for a cantilever beam problem shown in Fig. 5. The analytical solution has been given by Timoshenko and Goodier (1970) for the plane stress problem as follows

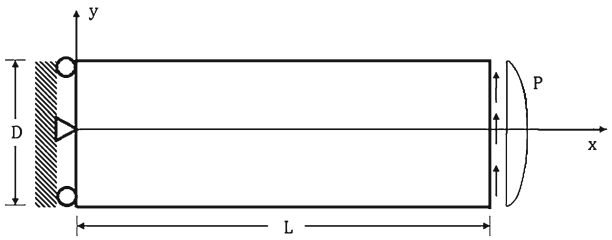

Fig. 5 Cantilever beam of unit width under the transverse distributed end load with the total of P

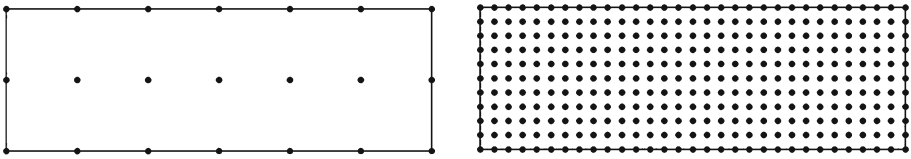

(a) 21 nodes **(b)** 341 nodes

Fig. 6 Regular nodal distribution for modeling the cantilever beam, AR = 1

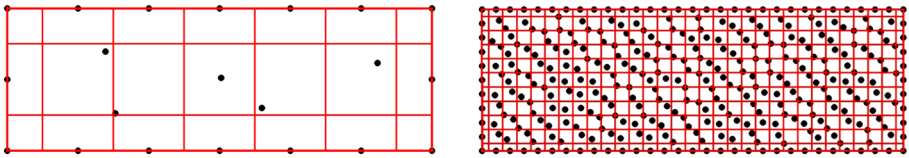

(a) 21 nodes **(b)** 341 nodes

Fig. 7 Background mesh with random nodal distribution for modeling the cantilever beam using MFV3

$$
\begin{aligned}
u_x &= -\frac{P}{6EI}\left[(6L-3x)x+(2+\nu)\left[y^2-\frac{D^2}{4}\right]\right]\\
u_y &= \frac{P}{6EI}\left[3\nu y^2(L-x)+(4+5\nu)\frac{D^2x}{4}+(3L-x)x^2\right]\\
\sigma_x &= -\frac{P(L-x)}{I}\\
\sigma_y &= 0\\
\tau_{xy} &= \frac{P}{2I}\left[\frac{D^2}{4}-y^2\right]
\end{aligned}
\tag{26}
$$

In the numerical model, the analytical displacement solution is prescribed at $x = 0$ and the exact shear traction is applied at $x = L$. The values for the geometry, material properties and loading are taken as $L = 3\,\text{m}$, $D = 1\,\text{m}$, $E = 1.0 \times 10^{10}\,\text{N/m}^2$, $\nu = 0.3$ and $P = 1000\,\text{N}$.

Five discretization levels with regular nodal positions are investigated for two aspect ratios (AR); see Fig. 6. Note that, AR is defined as the ratio of nodal space in x direction to the nodal space in y direction. It should be noted that the regular background mesh with random nodal distribution is used for MFV3 scheme. Two typical background meshes are shown in Fig. 7.

The vertical displacement along the neutral axis of the beam and the distribution of normal stress (σ_x) on a cross section at the left end of the beam obtained from MFV schemes with WMTM interpolation functions are plotted in Fig. 8. It can be observed that the displacements and stresses' results converge appropriately to the analytical solutions. For example, the displacement predictions converge to the analytical results when only 21 nodes are used.

Figures 9 and 10 show the convergence behavior of the presented MFV schemes in terms of the relative displacement and relative energy error norms corresponding to the different node numbers. A comparison between different MFV schemes and FEM shows that MFV2 scheme provides more accurate results in the prediction of relative displacement error norm for different aspect ratios. Also, according to Fig. 10, almost similar behaviors of MFV2 and FEM can be observed in predicting the relative energy error norm, corresponding to both cases of AR = 1 and AR = 10. As can be seen in Figs. 9 and 10, the convergence rate of the solutions obtained is also comparable with the first-order and second-order behaviors. It should be

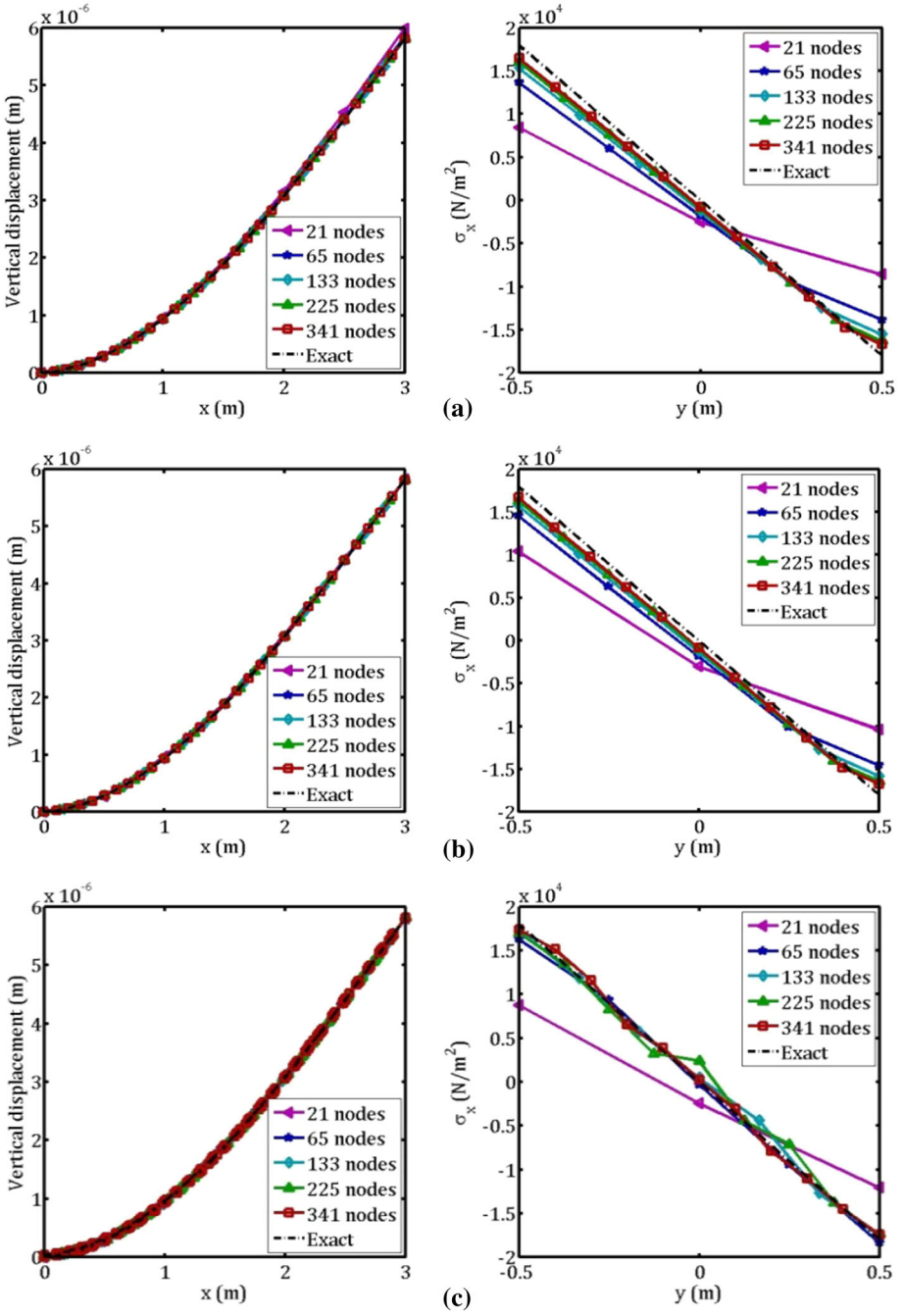

Fig. 8 The vertical displacement along the neutral axis of the beam and the normal stress (σ_x) at the left end of the beam obtained from WMTM-based MFV schemes (AR = 1), **a** MFV1, **b** MFV2 and **c** MFV3

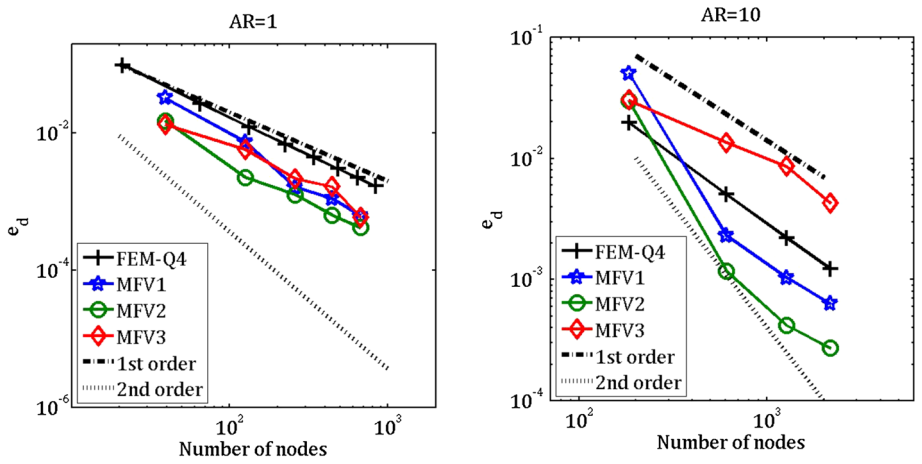

Fig. 9 Convergence of relative displacement norm obtained from WMTM-based MFV schemes with two aspect ratios for the cantilever beam problem

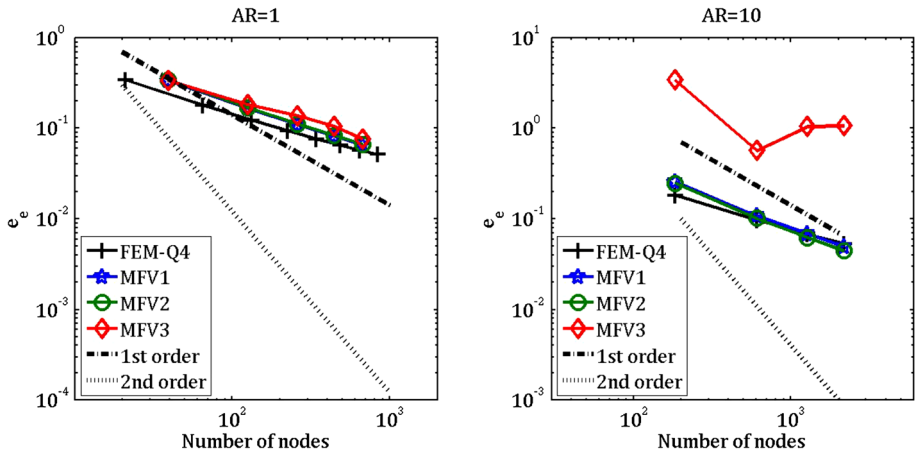

Fig. 10 Convergence of relative energy norm obtained from WMTM-based MFV schemes with two aspect ratios for the cantilever beam problem

mentioned that in MFV3 scheme, there is no dependence between the node locations and CVs construction, which can be the main reason for the poor performance of the MFV3 scheme.

According to these figures, the comparable capability of MFV1 and MFV2 schemes is demonstrated.

4.2 Infinite plate with a circular hole

In this benchmark problem, an infinite plate with a central circular hole of radius $a = 1$ m is investigated under the tension loading. Due to the symmetry, only one quarter with the edge length of 5 m is analyzed; see Fig. 11. The analytical solution for the plane stress condition is given as (Timoshenko and Goodier 1970)

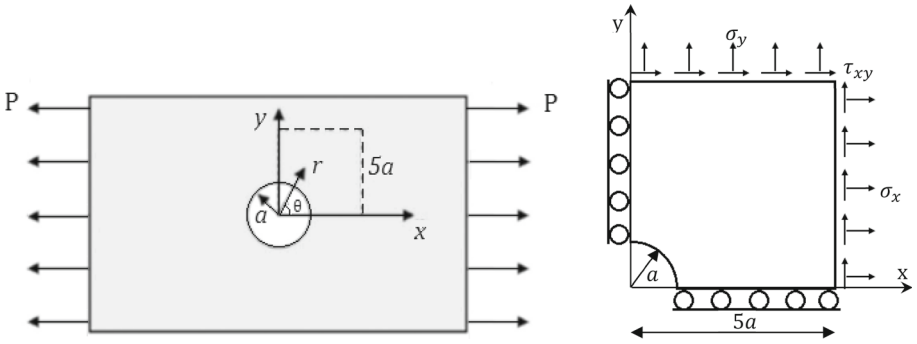

Fig. 11 Infinite plate with a circular hole

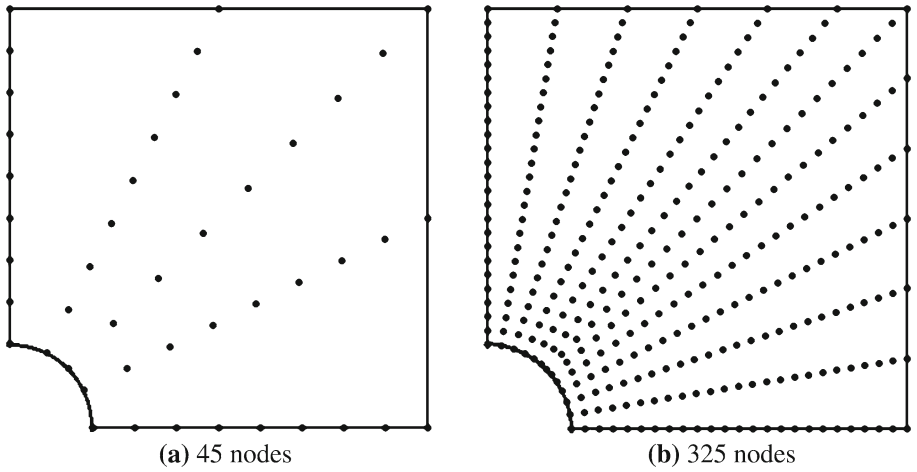

Fig. 12 Two nodal distributions for modeling of the infinite plate with a hole

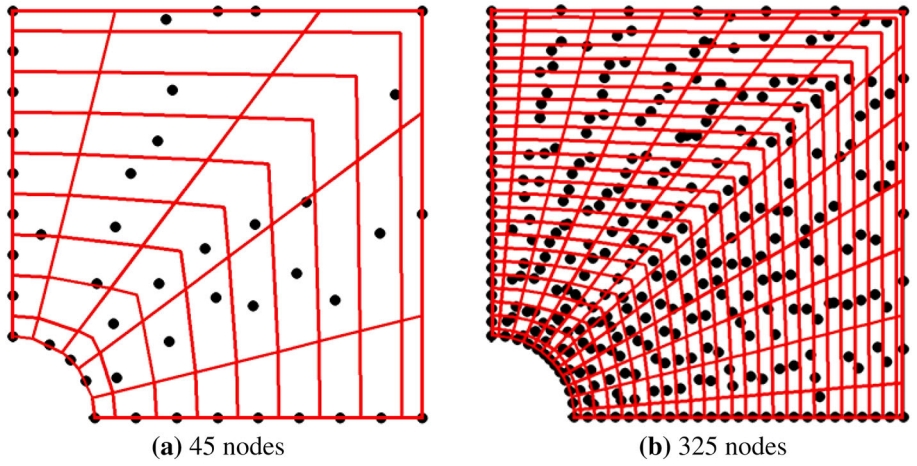

Fig. 13 Background mesh with random nodal distribution for modeling the infinite plate with a hole using MFV3

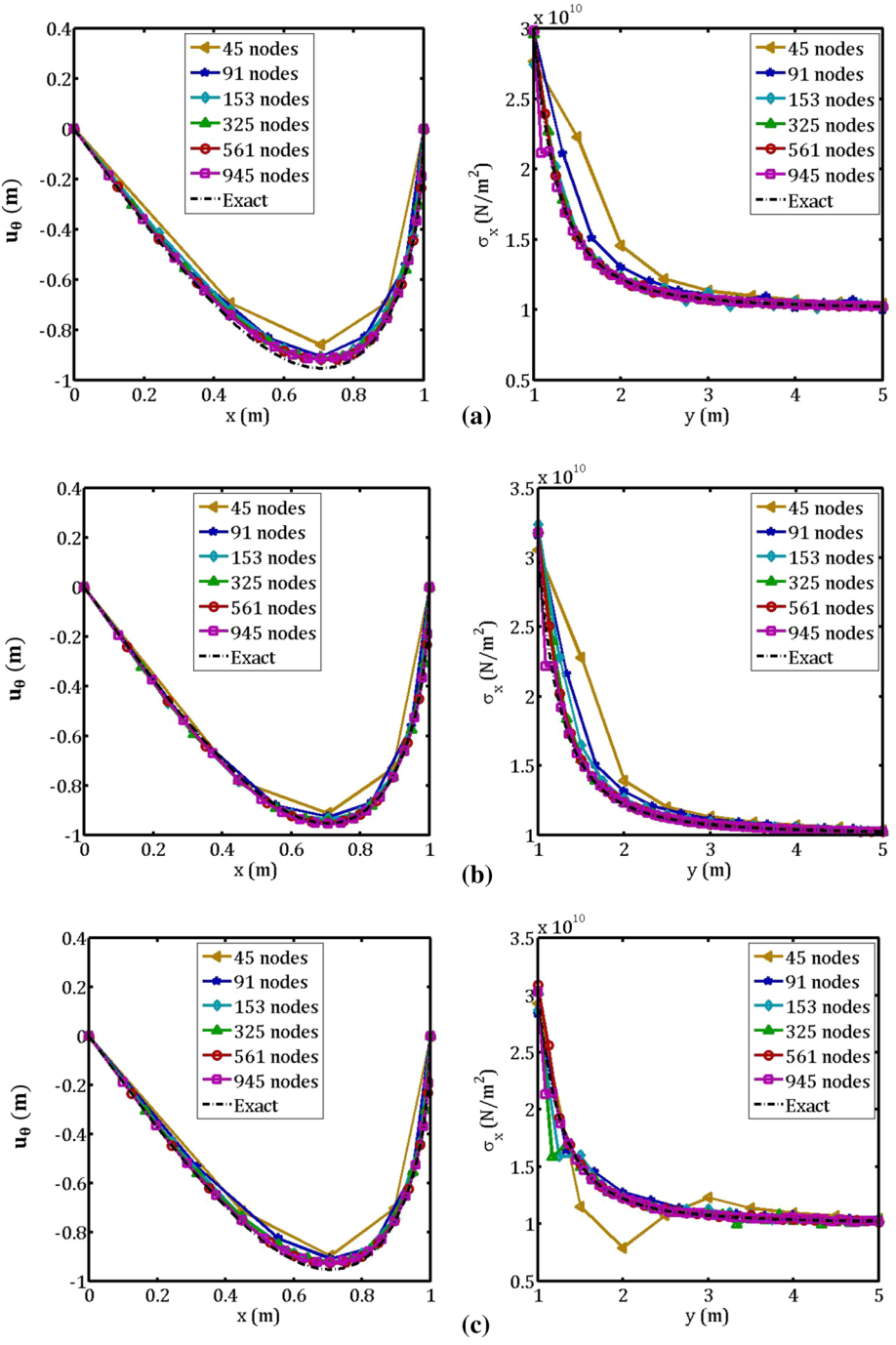

Fig. 14 The circumferential displacement along the hole and the normal stress (σ_x) at the left end obtained from WMTM-based MFV schemes, **a** MFV1, **b** MFV2 and **c** MFV3

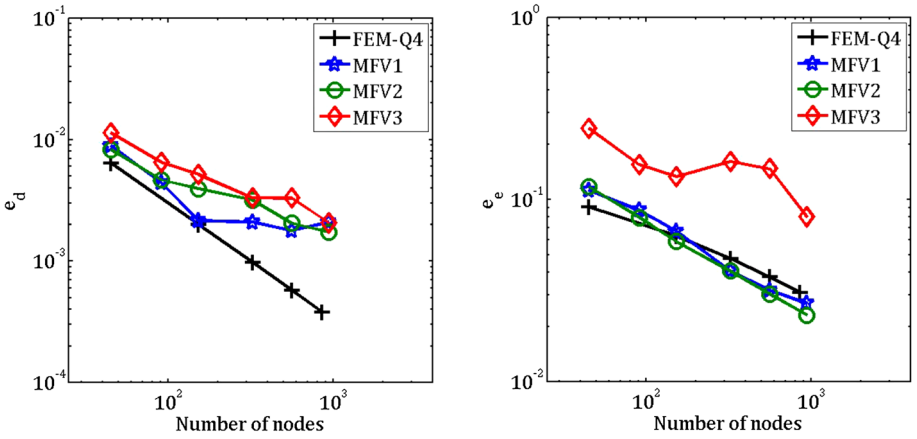

Fig. 15 Convergence of relative displacement and energy norms obtained from MFV schemes and FEM for the infinite plate with a circular hole

$$
\begin{aligned}
\sigma_x &= P\left\{1-\frac{a^2}{r^2}\left[\frac{3}{2}\cos(2\theta)+\cos(4\theta)\right]+\frac{3a^4}{2r^4}\cos(4\theta)\right\}\\
\sigma_y &= -P\left\{\frac{a^2}{r^2}\left[\frac{1}{2}\cos(2\theta)-\cos(4\theta)\right]+\frac{3a^4}{2r^4}\cos(4\theta)\right\}\\
\tau_{xy} &= -P\left\{\frac{a^2}{r^2}\left[\frac{1}{2}\sin(2\theta)+\sin(4\theta)\right]-\frac{3a^4}{2r^4}\sin(4\theta)\right\}\\
u_r &= \frac{P}{4G}\left\{r\left[\frac{\kappa-1}{2}+\cos(2\theta)\right]+\frac{a^2}{r}\left[1+(1+\kappa)\cos(2\theta)\right]-\frac{a^4}{r^3}\cos(2\theta)\right\}\\
u_\theta &= \frac{P}{4G}\left\{(1-\kappa)\frac{a^2}{r}-r-\frac{a^4}{r^3}\right\}\sin(2\theta)
\end{aligned}
\tag{27}
$$

where G is the shear modulus, ν represents the Poisson's ratio and $\kappa = 3-\nu/1+\nu$.

In the numerical model, the analytical displacement solutions are prescribed on the left and lower boundaries and the analytical tractions are applied on the upper and right boundaries of the solution domain.

The numerical analysis is carried out by investigating six different discretization levels with 45, 91, 153, 325, 561 and 945 nodes. Two typical nodal arrangements are shown in Fig. 12. For MFV3 scheme, the regular background meshes with random nodal distributions are used; see Fig. 13. In this problem, the uniform uniaxial traction, Young's modulus and Poisson's ratio are considered as, $P = 10^{10}\,\mathrm{N/m^2}$, $E = 10^{10}\,\mathrm{N/m^2}$ and $\upsilon = 0.3$, respectively.

Figure 14 shows the comparison between the exact and MFV values of normal stress (σ_x) predictions at the left end ($x = 0$) and also the tangential displacement along the hole. The solutions for all MFV schemes are in good agreement with the analytical solutions.

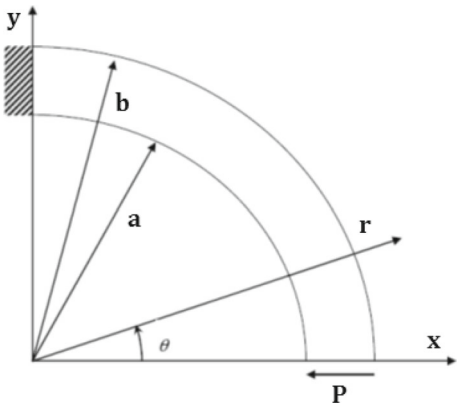

Fig. 16 Curved beam under bending

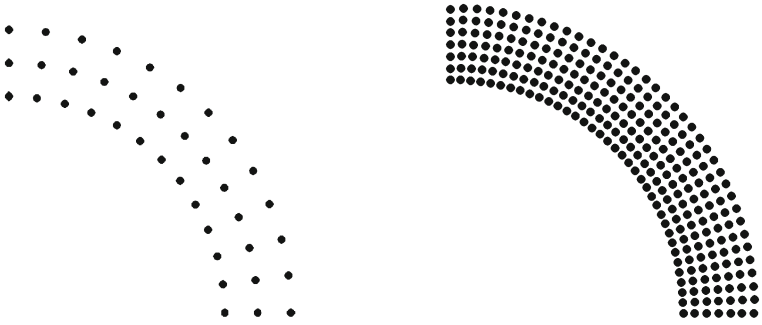

(a) 39 nodes **(b)** 259 nodes

Fig. 17 Two sample nodal distributions for curved beam problem

Finally, the relative displacement and energy error norms obtained by MFV schemes and FEM are compared in Fig. 15. It can be found that MFV2 scheme has better accuracy than MFV1, MFV3 and FEM in prediction of relative energy error norm. However, FEM shows better accuracy in prediction of relative displacement error norm.

4.3 Curved beam under bending

In the final example, the capability of different MFV schemes for the analysis of a curved beam under the bending loading (Fig. 16) is investigated. The curved beam is modeled with the unit thickness and $a = 13\,\text{m}$, $b = 17\,\text{m}$, the end load of $P = 1\,\text{N}$, the Young's modulus of $E = 1\,\text{N/m}^2$ and the Poisson ratio of $\nu = 0.25$. Different nodal distributions consist of 14, 39, 125, 259, 441, 671 and 949 nodes and are used in the numerical analysis. Two nodal arrangements which are used in MFV1 and MFV2 are shown in Fig. 17. For analyzing the curved beam using MFV3 scheme, the regular background mesh with random nodal distribution is used, as shown in Fig. 18.

The analytical solution for this problem has been given by Timoshenko and Goodier (1970) as

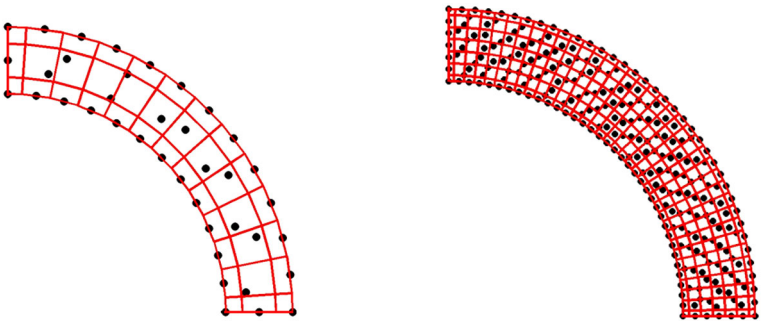

(a) 39 nodes **(b)** 259 nodes

Fig. 18 Background mesh with random nodal distribution for modeling the curved beam using MFV3

$$
\begin{aligned}
\sigma_r &= P\left(2Ar - \frac{2B}{r^3} + \frac{D}{r}\right)\sin\theta \\
\sigma_\theta &= P\left(6Ar + \frac{2B}{r^3} + \frac{D}{r}\right)\sin\theta \\
\sigma_{r\theta} &= -P\left(2Ar - \frac{2B}{r^3} + \frac{D}{r}\right)\cos\theta \\
u_r &= \frac{P}{E}\left[-2D\theta\cos\theta + \sin\theta\left(D(1-\nu)\log r + A(1-3\nu)r^2 + \frac{B(1+\nu)}{r^2}\right)\right. \\
&\quad \left. + K\sin\theta + L\cos\theta\right] \\
u_\theta &= \frac{P}{E}\left[2D\theta\sin\theta - \cos\theta\left(-D(1-\nu)\log r + A(5+\nu)r^2 + \frac{B(1+\nu)}{r^2}\right)\right. \\
&\quad \left. + D(1+\nu)\cos\theta + K\cos\theta - L\sin\theta\right] \\
N &= a^2 - b^2 + (a^2+b^2)\log\frac{b}{a} \\
A &= \frac{1}{2N},\ B = -\frac{a^2b^2}{2N},\ D = -\frac{a^2+b^2}{N},\ L = D\pi \\
K &= -\left(D(1-\nu)\log r_0 + A(1-3\nu)r_0^2 + \frac{B(1+\nu)}{r_0^2}\right),\quad r_0 = \frac{a+b}{2}
\end{aligned}
\tag{28}
$$

For the comparison purposes, the tangential displacement, u_θ, along the line $\theta = 0$ and the distribution of hoop stress σ_θ along the line $\theta = \pi/4$ are obtained from MFV schemes and compared with the exact solutions in Fig. 19. It can be observed that the proposed methods are able to predict results that converge to the analytical solutions.

Finally, the convergence and the accuracy of different MFV schemes are shown in Fig. 20 and compared with the FEM results corresponding to the different discretization levels. This figure shows that the proposed MFV schemes lead to the much more accurate results than FEM. Moreover, it reveals that the proposed MFV schemes are in the same order of accuracy for this example.

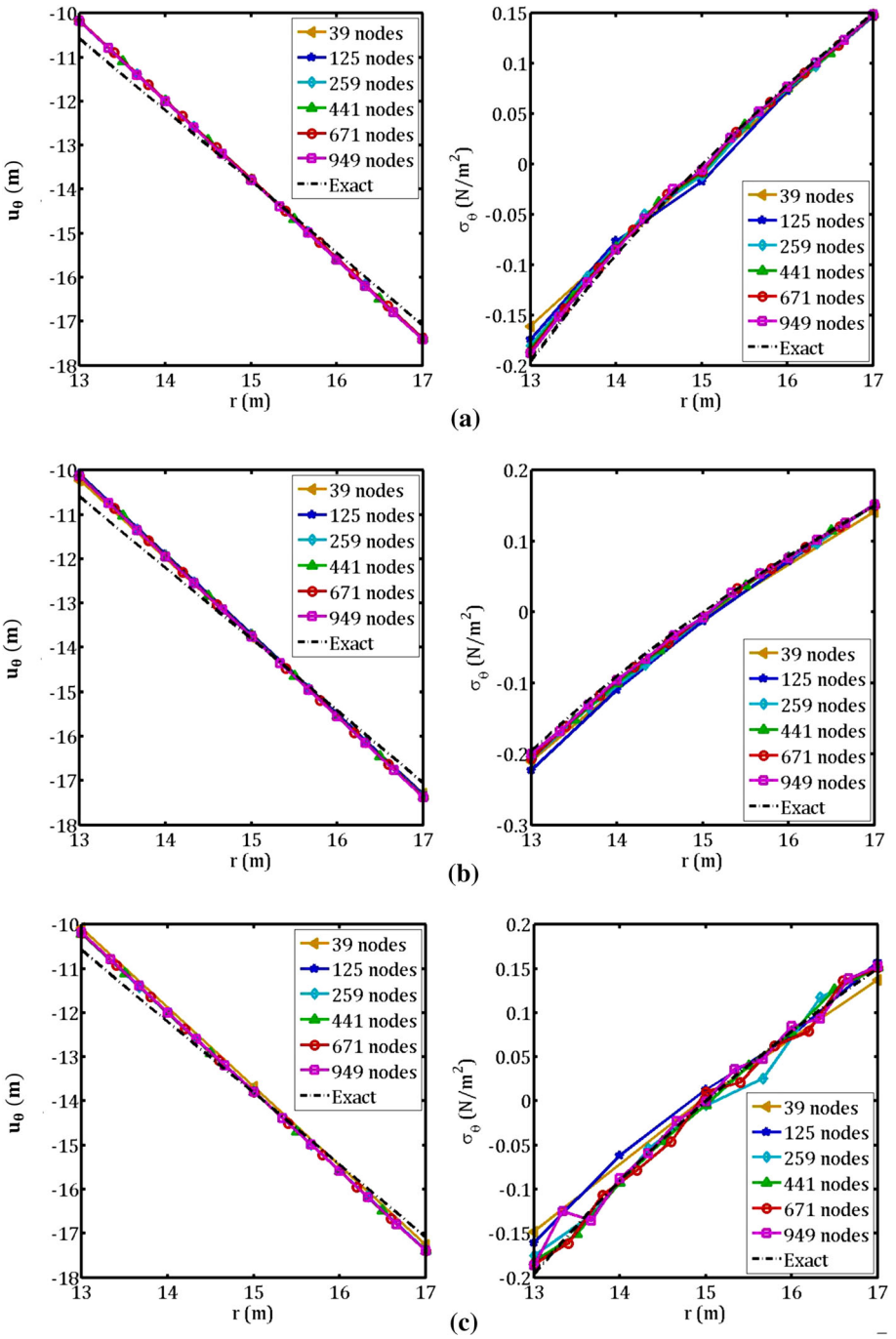

Fig. 19 The tangential displacement along the free end and the hoop stress σ_θ at $\theta = \frac{\pi}{4}$ for the curved beam obtained from WMTM-based MFV schemes, **a** MFV1, **b** MFV2 and **c** MFV3

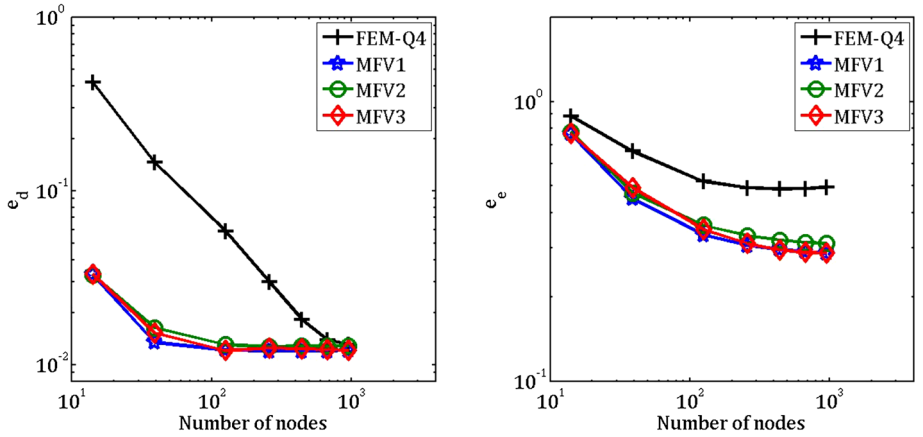

Fig. 20 Convergence of relative displacement and energy norms obtained from WMTM-based MFV schemes for the curved beam problem

5 Conclusions

In this paper, a class of different two-dimensional MFV methods based on the WMTM interpolation functions has been presented. WMTM-based MFV schemes show significant advantages over the other meshless methods, where the domain integrals for the stiffness matrix calculations are eliminated and the integration is only implemented over the CVs boundaries using Gaussian quadrature rule. Moreover, the domain of influence of a field node depends only on the positions of the neighbor nodes determined through a Delaunay triangulation of the domain. The proposed MFV1 and MFV2 schemes utilize the node-dependent CVs, while MFV3 scheme eliminates dependency of the field node positions and CVs construction.

Analysis of two-dimensional elasticity problems by MFV schemes with WMTM interpolation functions leads to high accuracy results. In most of the considered problems, it can be observed that the results obtained by MFV1 and MFV2 schemes are more accurate than MFV3 and FEM. Although MFV3 is not as accurate as MFV1 and MFV2, however, its special feature to construct the simple geometry CVs regardless of the position of field nodes makes it attractive for the analysis of problems with complex geometries.

References

Atluri SN, Zhu T (1998) A new meshless local Petrov–Galerkin (MLPG) approach in computational mechanics. Comput Mech 22:117–127

Atluri SN, Shen S (2002) The meshless local Petrov–Galerkin (MLPG) method: a simple and less costly alternative to the finite element and boundary element methods. Comput Model Eng Sci 3(1):11–52

Atluri SN, Han ZD, Rajendran AM (2004) A new implementation of the meshless finite volume method through the MLPG mixed approach. Comput Model Eng Sci 6(6):491–513

Bailey C, Cross M (1995) A finite volume procedure to solve elastic solid mechanics problems in three dimensions on an unstructured mesh. Int J Numer Meth Eng 38:1756–1776

Belytschko T, Lu YY, Gu L (1994) Element-free Galerkin methods. Int J Numer Meth Eng 37:229–256

Demirdzic I, Martinovic D (1993) Finite volume method for thermo-elasto plastic stress analysis. Comput Meth Appl Mech Eng 109:331–349

Ebrahimnejad M, Fallah N, Khoei AR (2014) New approximation functions in the meshless finite volume method for 2D elasticity problems. Eng Anal Bound Elem 46:10–22
Fallah NA, Bailey C, Cross M, Taylor GA (2000) Comparison of finite element and finite volume methods application in geometrically nonlinear stress analysis. Appl Math Model 24:439–455
Fallah N (2004) A cell vertex and cell centered finite volume method for plate bending analysis. Comput Meth Appl Mech Eng 193:3457–3470
Fallah N (2006) On the use of shape functions in the cell centered finite volume formulation for plate bending analysis based on Mindlin–Reissner plate theory. Comput Struct 84:1664–1672
Fallah N, Hatami F (2006) A displacement formulation based on finite volume method for analysis of Timoshenko beam. In: Proceedings of the 7th international conference on civil engineering, Tehran, Iran
Fallah N, Ebrahimnejad M (2014) Finite volume analysis of adaptive beams with piezoelectric sensors and actuators. Appl Math Model 38(2):722–737
Fallah N, Paryandeh-Shahrestany A (2014) A novel finite volume based formulation for the elasto-plastic analysis of plates. Thin Wall Struct 77:153–164
Ganzenmüller GC, Hiermaier S, May M (2015) On the similarity of meshless discretizations of Peridynamics and Smooth-Particle Hydrodynamics. Comput Struct 150:71–78
Han ZD, Atluri SN (2004a) Meshless local Petrov–Galerkin (MLPG) approaches for solving 3D problems in elasto-statics. Comput Model Eng Sci 6(2):169–188
Han ZD, Atluri SN (2004b) A meshless local. Petrov–Galerkin (MLPG) approaches for solving 3-dimensional elasto-dynamics. Comput Mater Con 1(2): 129–140
Ivankovic A, Demirdzic I, Williams JG, Leevers PS (1994) Application of the finite volume method to the analysis of dynamic fracture problems. Int J Fract 66(4):357–371
Khoei AR, Samimi M, Azami AR (2007) Reproducing kernel particle method in plasticity of pressure sensitive material with reference to powder forming process. Comput Mech 39:247–270
Liu WK, Jun S, Zhang YF (1995) Reproducing kernel particle methods. Int J Numer Meth Eng 20:1081–1106
Liu G, Liu M (2003) Smoothed particle hydrodynamics: a meshfree particle method. World Scientific, Singapore
Maneeratana K (2000) Development of the finite volume method for non-linear structural applications. Dissertation, Imperial College, University of London
Moosavi MR, Delfanian F, Khelil A (2011) Orthogonal meshless finite volume method in elasticity. Thin Wall Struct 49(6):708–712
Moosavi MR, Delfanian F, Khelil A (2012a) Orthogonal meshless finite volume method in shell analysis. Finite Elem Anal Des 62:1–7
Moosavi MR, Delfanian F, Khelil A (2012b) Orthogonal meshless finite volume method applied to crack problems. Thin Wall Struct 52:61–65
Oñate E, Idelsohn S, Zienkiewicz OC, Taylor RL (1996) A finite point method in computational mechanics: applications to convective transport and fluid flow. Int J Numer Meth Eng 139:3839–3866
Qian LF, Batra RC, Chen LM (2003) Elastostatic deformations of a thick plate by using a higher order shear and normal deformable plate theory and two meshless local Petrov–Galerkin (MLPG) methods. Comput Model Eng Sci 4(1):161–176
Raju IS, Phillips DR (2003) Further developments in the MLPG method for beam problems. Comput Model Eng Sci 4(1):141–160
Sabbagh-Yazdi SR, Mohammadzadeh-Qomi M (2004) Finite volume solution of two-dimensional convection dominated sub-critical free surface flow using unstructured triangular meshes. Int J Civil Eng 2(2):78–91
Silling SA, Epton M, Weckner O, Xu J, Askari E (2007) Peridynamic states and constitutive modeling. J Elast 88:151–184
Slone AK, Bailey C, Cross M (2003) Dynamic solid mechanics using finite volume methods. Appl Math Model 27:69–87
Stylianou V, Ivankovic A (2002) Finite volume analysis of dynamic fracture phenomena. Int J Fract 113:107–123
Taylor GA, Bailey C, Cross M (2003) A vertex-based finite volume method applied to non-linear material problems in computational solid mechanics. Int J Numer Meth Eng 56:507–529
Timoshenko SP, Goodier JN (1970) Theory of elasticity. McGraw-Hill, New York
Wheel MA (1996) Geometrically versatile finite volume formulation for plane strain elastostatic stress analysis. J Strain Anal Eng Des 31:111–116
Wheel MA (1997) A finite volume method for analyzing the bending deformation of thick and thin plates. Comput Meth Appl Mech Eng 147:199–208